Medium-Scale Travelling Ionospheric Disturbances Studied with the TIGER HF SuperDARN Radar

Longsong HE, Peter DYSON, Murray L. PARKINSON, Phillip J. WILKINSON, and Weixing WAN

***Abstract*—A cross-spectral Fourier transform method has been applied to TIGER HF radar observations to determine propagation velocities of medium-scale travelling ionospheric disturbances (MSTIDs). Observations of numerous MSTIDS during a 12-day winter interval showed consistent MSTID propagation directions during the day which changed from northeast to northwest around 0500 UT (~1500 Magnetic Local Time). It is suggested that this change was related to fore- and after-noon maxima in the distribution of field-aligned currents flowing from the magnetosphere to the ionosphere, and that these two regions were sources of atmospheric gravity waves (AGWs) due to Joule heating caused by the subsequent horizontal currents flowing in the E region. It is speculated the change in propagation direction was also controlled by thermospheric neutral winds Doppler-shifting the AGWs in proximity to the source regions.**

***Index Terms*—Fourier transform, travelling ionospheric disturbances, atmospheric gravity waves, HF propagation, SuperDARN radars**

I. Introduction

SuperDARN radars are powerful instruments for studying medium-scale travelling ionospheric disturbances (MSTIDs) through the detection of focusing and defocusing of radar signals propagated via the ionosphere and backscattered by land or sea [1], [2], [3]. The waxing and waning of ground- and sea-echo power produces a characteristic periodic MSTID pattern or signature in range-time plots of echo power. Related but weaker signatures also occur in other echo parameters including the Doppler shift and Doppler spectral width. This study uses observations by the Tasman International Geospace Environment Radar (TIGER) [4], a component of the SuperDARN network, to determine properties of MSTIDs. Since TIGER's footprint maps almost entirely over the Southern Ocean, we use the term "sea echoes" to refer to the echoes back-scattered from the Earth's surface.

MSTIDs are thought to be an ionospheric manifestation of atmospheric gravity waves (AGWs) propagating through the thermosphere. The Doppler shifts measured by HF backscatter radars are due to the motion of ionospheric irregularities perpendicular to the magnetic field lines. Thus AGWs must transport field-perpendicular electric fields for their signatures to manifest in the Doppler shifts of ionospheric scatter. Although this may happen, so far the effect has proven difficult to detect amidst the numerous perturbations of magnetospheric origin. Hence in this paper we concentrate on the analysis of MSTID signatures in the sea-echo powers.

Many data analysis methods have been developed to determine MSTID and AGW parameters including the phase velocity, azimuth, and wavelength from different types of radio observations [5], [6], [7], [8]. For example, Tsutsui et al. [5] developed a cross spectral Fourier transform technique to determine wind velocity from an HF radar array, and Shibata [7] and Wan et al. [8] applied the maximum entropy method in their MSTID studies using radio systems. In analyzing SuperDARN observations to detect MSTID excitation sources, Samson et al. [2] applied a cross-spectral analysis method ("MUSIC") to time series obtained at different range gates using the Goose Bay radar.

SuperDARN radars measure the group range, backscatter power, line-of-sight Doppler velocity, and spectral width of sea echoes. In principle, reasonably accurate propagation models can be used to convert the group range to estimates of the true ground range. However, this is generally not the range at which any ionospheric effects, such as those due to MSTIDs, are imposed on the sea echoes. If there are no large horizontal gradients in the ionosphere, then any major ionospheric effects on the signal will be imposed near the ionospheric reflection height located at half the sea-echo range. This factor of $r = 1/2$ was used by Bristow et al. [3] in deducing MSTID propagation properties from SuperDARN data. However, Hall et al. [9] argued from their ray-tracing studies that horizontal gradients were significant, and the most suitable factor was 1/1.66. In contrast, MacDougall et al. [10] deduced the appropriate factor was closer to 1.0. This uncertainty is considerable, but it should be noted it does not affect the determination of the MSTID propagation directions which are a major focus of this paper.

This work was supported by the Australian Research Council, the Antarctic Science Advisory Council, and members of the TIGER consortium.

L.-S. He, P. L. Dyson, and M. L. Parkinson are with the Department of Physics, La Trobe University, Bundoora, Victoria 3086, Australia. L.-S. He was on leave from the Polar Research Institute of China, Shanghai 200129, China (e-mail: l.he@latrobe.edu.au; p.dyson@latrobe.edu.au).

P. J. Wilkinson is with IPS Radio and Space Services, Sydney, New South Wales 1240, Australia (e-mail: phil@ips.gov.au).

W. Wan is with the Wuhan Institute of Physics, Academic Sinica, Wuhan 430071, China (e-mail: wwx@wipm.whcnc.ac.cn).

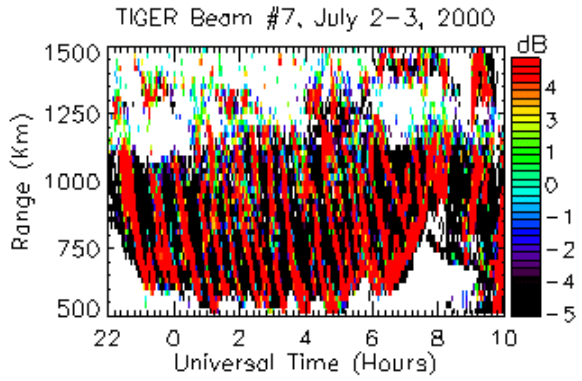

Fig. 1. Range-time plot of sea-echo power recorded using TIGER beam 7 from 2200 UT on 2nd July to 1000 UT on 3rd July, 2000. The powers were band-pass filtered over the period range 10 to 100 min. Magnetic latitudes of 60°, 65°, and 70°S correspond to ranges 486, 1041, and 1581 km, respectively. An HF propagation factor, r = 0.5, was used in all of the calculations in this paper.

Here, we present a new method for determining MSTID propagation speeds and azimuths using TIGER observations. The method is based on that of Tsutsui et al. [5] developed for use with an HF Doppler array. The method has been used here to study variations in the propagation direction of MSTIDs during an interval of austral winter.

II. Instrument

TIGER [4] is located on Bruny Island (43.4°S, 147.2°E geographic), Tasmania. Like other SuperDARN radars, it uses an array of 16 log-periodic antennas, operates in the frequency range 8 to 20 MHz, and covers 52º of azimuth by sequentially stepping through 16 beam directions [11]. In the routine mode of operation, TIGER normally performs one full-scan every 2 min, but in the high time resolution mode each beam is sampled every 1 min. Here we use Universal Time (UT) as the primary time reference because local time varies across the TIGER footprint and along most of the individual beams. Note, however, that local time is of the order of UT plus 10 hours. In terms of the observation of first-hop F-region sea echoes, local daytime corresponds to the interval ~2200 to 0800 UT during winter. TIGER is located at a lower latitude than any other operational SuperDARN radar providing an opportunity to extend SuperDARN measurements of TIDs to subauroral latitudes.

III. TID Propagation

A. Data Presentation

Fig. 1 shows a range-time plot of sea-echo power observed along beam 7 from 2200 to 1000 UT during 2 to 3 July, 2000, corresponding to local daytime hours. MSTIDs are clearly evident in the form of sloping quasi-periodic power enhancements that move toward the radar with time. MSTID signatures are weaker in range-time plots of Doppler velocity, and weaker again in range-time plots of spectral width. Thus we only use the sea-echo powers in the present analysis, but work continues on understanding the relationship between the signatures in different parameters.

The sea-echo powers were filtered to accentuate the presence of MSTIDs using a familiar technique: the time series at each range gate were Fourier-transformed to the frequency domain and a band-pass filter was applied by setting frequency components outside the band pass to zero. This filtered frequency spectrum was then transformed back to the time domain to give the filtered time series. For Fig. 1, the band-pass filter covered the period range 10 to 100 min. This band-pass filter was used throughout the study because it rejected Pc 5 hydromagnetic wave activity with periods <10 min, whilst encompassing 20 to 50 min, the periods of most MSTIDs detected by SuperDARN radars [3].

B. Data Analysis Method

The primary aim of the analysis was to determine the velocities of MSTIDs propagating through the TIGER field of view. This required the MSTID frequency (or period) and wavelength (or wavenumber) to be determined from time series of sea echoes. Sea echoes were identified using the standard SuperDARN analysis algorithm which identifies "ground echoes" when their line-of-sight Doppler velocity and spectral widths are less than 50 m s^{-1} and 20 m s^{-1}, respectively. This algorithm is usually very effective in separating sea echoes from ionospheric echoes.

We chose time series of length 4 hours to estimate the MSTID frequencies, as this matched the approximate duration over which the coherency of the dominant wave trains was maintained. The chosen time window was stepped at ten-minute intervals through longer data sequences in order to detect MSTIDs as they occurred. Note that because of the finite coherency lengths of MSTIDs, increasing or decreasing the chosen time-series length increased the sensitivity of the power spectra to waves of longer or shorter period, respectively.

The first stage of the analysis was to identify the periodic variations consistent with MSTIDs at each range gate on every beam (which we call "observation cells"). An observation cell was included in the analysis if and when it provided a nearly continuous 4-hour time series of sea-echoes. Each 4-hour time series of sea-echo power was converted to a time series of amplitude and then Fourier-transformed and band-pass filtered, as explained in the previous section. For a given time window, sea echoes often occurred at many observation cells, so this first stage of analysis generally produced numerous power spectra for further analysis.

For the next stage of analysis, we developed a cross spectral analysis method to identify, for a given time window, the two-dimensional wave numbers of MSTIDs appearing across the full radar field of view.

Let $\boldsymbol{k} = (k_x, k_y)$ represent an AGW of wave number $\boldsymbol{k}$ propagating across the TIGER field of view. The positive y axis is taken to be in the direction of geographic south, which is mid-way between beams 7 and 8. Likewise, the x axis is taken as positive towards the east, and the origin of both axes was located at zero range. In order to simplify the calculations, the MSTIDs were regarded as isolated, single wave packets.

The spectral amplitudes were used as weighting factors in the calculations.

For a time window centered on a time, τ, and for a specific observation cell (beam number and range) denoted by indices (b, r), the frequency spectrum of the associated fluctuations observed by the radar, $\boldsymbol{A}_{b,r,\tau}(\omega)$, can be written as

$$\boldsymbol{A}_{b,r,\tau}(\omega) = A_{b,r,\tau}(\omega)\, e^{-i(k_x x + k_y y)} \quad (1)$$

where $b = 1, 2, 3, \ldots$; $r = 1, 2, 3, \ldots$
and $b_{max} \le 16$, $r_{max} \le 75$

The corresponding cross-spectra $\boldsymbol{\phi}_{b,r,b',r',\tau}(\omega)$ of fluctuations between the reference cell (b, r) and adjacent observation cells (b', r') are given by:

$$\boldsymbol{\phi}_{b,r,b',r',\tau}(\omega) = \phi_{b,r,b',r',\tau}(\omega)\, e^{-i(k_x(x_r - x_{r'}) + k_y(y_b - y_{b'}))} \quad (2)$$

$$\boldsymbol{\phi}_{b,r,b',r',\tau}(\omega) = \boldsymbol{A}_{b,r,\tau}(\omega)\, \boldsymbol{A}^{*}_{b',r',\tau}(\omega) \quad (3)$$

Hence the difference between the phases (i.e., the cross phases given in (2)) of every permutation of three non-collinear cells was then calculated. The orthogonal distances between the centre of cells, Δx and Δy, were calculated using spherical trigonometry to allow for the spreading of the beams with range. The meridional and zonal wave numbers were then obtained (i.e., $k_x = \Delta\phi_x/\Delta x$ and $k_y = \Delta\phi_y/\Delta y$). A histogram showing the number of permutations at a particular wave number was then used to identify the dominant wave vectors. In practice, the calculations were only performed at the relatively few MSTID wave periods given by the dominant spectral peaks within the power spectra.

In order to prevent spatial aliasing, a maximum range separation between cells was set for use in the three-cell analysis; otherwise aliasing in the form of 2π phase ambiguities occurred. The wavelengths of MSTIDs were usually >200 km, so restricting the wave-vector analysis to cells adjacent in range (45 km) eliminated aliasing, except for wave numbers $>70 \times 10^{-6}$ m^{-1}.

Finally, the determination of the MSTID wave period and orthogonal wave-vector components enabled the calculation of the phase velocity:

$$V_{ph} = \omega(k_x^2 + k_y^2)^{-1/2} \quad (4)$$

and the wave propagation direction:

$$Az = tan^{-1}(k_y/k_x) \quad (5)$$

Application of this cross-spectral analysis method permitted recovery of the two-dimensional MSTID dispersion and can lead to an intimate understanding of the spatial and temporal coherency of MSTIDs appearing across the radar field of view.

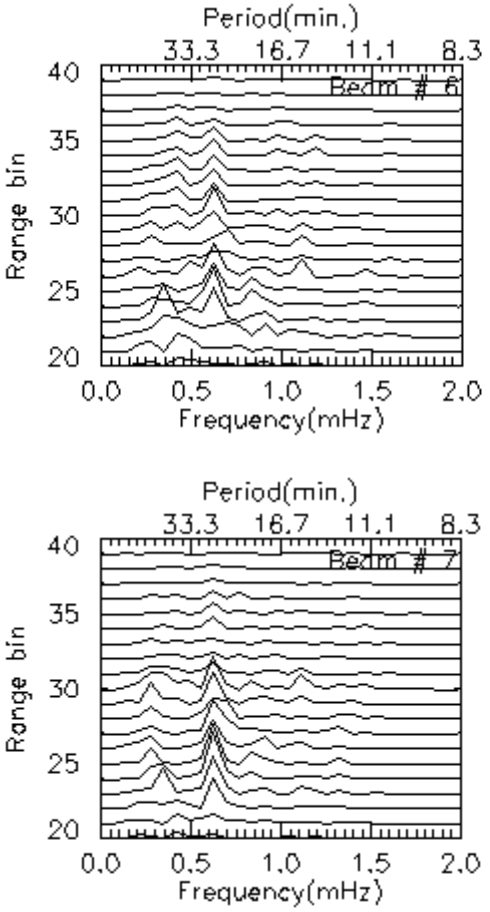

Fig. 2. Stack plots of power spectra calculated for range gates 20 to 40 along beams 6 (upper) and 7 (lower). The frequency resolution of these spectra is 0.069 mHz, and the scale for spectral power is 2.5×10^5 Counts^2 mHz^{-1} per range bin. A dominant MSTID with a period of 27 min is clearly seen.

C. A Case Study: TID Events on 2nd to 3rd July, 2000

Fig. 2 shows power spectra of the time series of sea-echo amplitude recorded during 0000 to 0400 UT at a number of range gates along beams 6 and 7 (cf., Fig. 1). The dominant feature in both spectra is a spectral peak, well above the background noise, at a period of 27 min (frequency 0.62 mHz), and appearing in range gates 20 to 40 (ranges 540 to 1980 km). Some spatial incoherency across the field of view was evident since spectral peaks appeared at other frequencies on different beams. In the following calculations, beam 7 was used as a reference beam, i.e., only the dominant periods occurring in beam 7 frequency spectra were used in the calculations. The phase velocity and azimuth were estimated using equations (4) and (5) applied to non-collinear cells, as explained above. The results, when plotted as a histogram, identified the most coherent waves moving across the field of view.

Fig. 3 shows histograms of the two orthogonal components of horizontal wave numbers k_x and k_y derived in this manner at a period of 27 ± 1.5 min. An HF propagation factor, $r = 0.5$ was used in the calculations. The mode values in the distributions of k_x and k_y were $(12 \pm 0.002) \times 10^{-6}$ m^{-1} and $-(15 \pm 0.002) \times 10^{-6}$ m^{-1}, respectively, with the uncertainties deter-

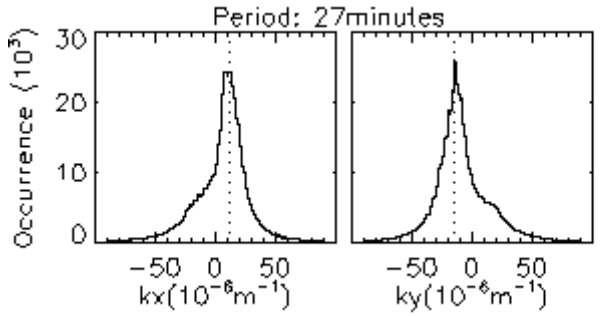

Fig. 3. Distributions of MSTID wave number vector, k_x (left) and k_y (right) at a period of 27 min. The mode values of the distributions are used to estimate the MSTID wavelengths, phase velocities, and azimuth angles. An HF propagation factor, $r = 0.5$, was used in the calculations.

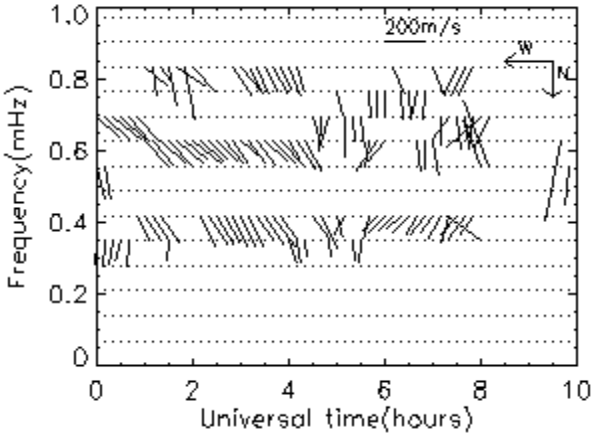

Fig.4. Phase velocity plots in the frequency-time plane. All of the vectors point northward (equatorward), but they changed from northeast to northwest at about 0500 UT.

mined by the bin size of wave number. Hence the estimated wavelength of the dominant wave component was 327 ± 0.05 km, and, using equations (4) and (5), the estimated phase velocity was 203 ± 11 m s^{-1}. If the MacDougall et al. (2001) HF propagation factor, r =1, is considered, the phase velocity increases from 203 m s^{-1} (r = 1/2) to 406 m s^{-1} (r = 1). The azimuthal angle was 309° (i.e., northeast), and unaffected by the chosen value of r. Broad humps around $k_x = -20 \times 10^{-6}$ m^{-1} and $k_y = 20 \times 10^{-6}$ m^{-1} can also be seen in Fig. 3, and were caused by poleward propagating features of wavelength ~222 km.

Fig. 4 shows the variation in phase velocity with time calculated for the interval 2nd to 3rd July, 2000. The behaviour of the dominant wave number at each frequency identified by the mode values in analyses similar to Fig. 3 are shown. It is evident that at least two long lasting, trends were detected. The estimated phase velocity was mostly in the range 200 to 250 m s^{-1} (r = 1/2). At 0.42 mHz, the azimuth angles were clearly northeast prior to 0500 UT, after which they changed to northwest. At 0.62 mHz, the azimuth angles were northeast from 0100 to 0500 UT, and thereafter became erratic, but trended toward the northwest.

Mean hourly values of phase speed and azimuth have been determined for each hour of the day and these are shown in

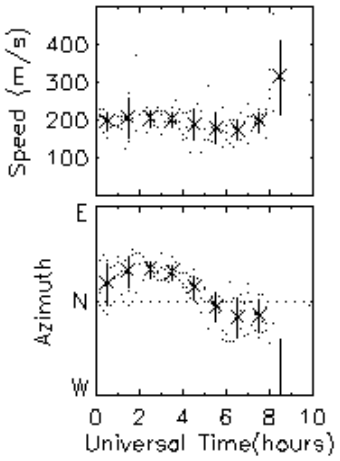

Fig. 5. The velocities at the same frequencies shown in Fig. 4, except the speed and azimuth have been separated: phase velocity (upper), azimuth angle (lower). The mean values and scatter bars (± 1 standard deviation) are given for every 1-hour interval.

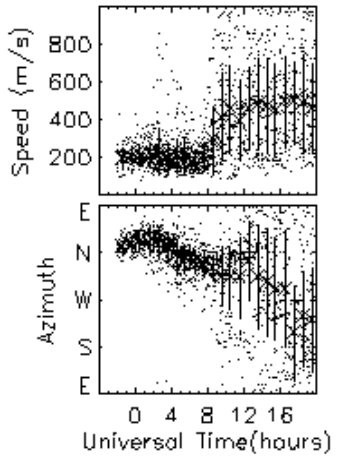

Fig. 6. The distribution of phase speed (upper) and azimuth angle (lower) during the winter of 2000. The mean values and scatter bars (± 1 standard deviation) are given for every 1-hour interval.

Fig. 5. It is evident the phase speeds were relatively constant at about 200 m s^{-1}, but with a slight decrease after 0500 UT. The azimuths indicate propagation towards the northeast before 0500 UT and a sudden increase at 0830 UT, with a subsequent, gradual change to the northwest and a further sudden change at 0830 UT.

D. TID propagation during Winter

Fig. 6 shows a summary of numerous MSTIDs observed during a 12-day interval in June and July 2000 when very distinct MSTID wave trains occurred, usually during geomagnetic quiet conditions [12]. These events were identified using TIGER beam 7 as a reference beam for the choice of dominant spectral peaks for further analysis. The main features evident in these mass plots are in fact similar to the main features shown in the case study, Fig. 5. From 2200 to 1000 UT, corresponding to daytime hours of ~0800 to 2000 LT, the wave speeds were typically 200 m s^{-1}. During the rest of the day, i.e., the local night, the observations were very scattered, but the average speeds were in the vicinity of 400 to

500 m s^{-1}, approaching the upper limit expected for MSTIDs.

The propagation directions tended to change from predominantly northward (equatorward) during the day, to scattered but predominately southward (poleward) past midnight. Recall the directions changed from an initial northeast direction to northwest at around 0500 UT (~1500 LT). It is interesting that northwest propagation directions prevail during the evening at mid-latitudes [13], [14].

The equatorward boundary of auroral and subauroral activity often expands equatorward of the sea echoes detected by TIGER after midnight [15]. Hence it is likely TIGER will begin to detect the effects of poleward propagating AGWs known to inhabit the polar cap ionosphere past midnight [16], [17].

IV. Discussion and Conclusions

Observations of MSTIDs using SuperDARN radars are controlled by the product of various factors including the manifestation of AGW excitation regions, conditions affecting the propagation of the AGWs, and conditions affecting the observations of sea echoes. For example, our observations show a strong daytime bias when almost continuous sea echoes are observed, whereas ionospheric echoes often prevail during the night. Obtaining first-hop sea echoes during the night also relies on HF propagation via auroral- and sporadic E-layers, and F layers enhanced by geomagnetic activity [18].

The difficulty of observing AGWs during the night might also be compounded because the wave fields become intrinsically less coherent in proximity to source locations near the auroral oval. In general, the wave field probably becomes less coherent when geomagnetic disturbances generate numerous AGWs with different phase speeds propagating in different directions [12]. The signatures of MSTIDs in SuperDARN radars are probably also biased toward geomagnetic quiet conditions because the AGW amplitudes are attenuated by the increase in upper atmosphere neutral particle densities with geomagnetic activity [19].

The technique using Fourier transform and cross-spectral analyses that we have developed for use with SuperDARN sea-echo data to identify the properties of MSTIDs assumes reasonably coherent wave fields. In this method, one must allow for the possibility that the power of each Fourier component was not due entirely to a single wave, i.e., there may be contributions from waves propagating in other directions. However, Fig. 1 clearly showed the propagation of the dominant wave components, and the corresponding parameters estimated by our method were reasonable after the effect of the HF propagation factor, r, was considered. In our calculations, we favoured the simple use of $r = 1/2$ given by Bristow et al. [3]. This enabled us to estimate a dominant wavelength of 327 ± 0.05 km and phase velocity of 203 ± 11 m s^{-1} at the period with greatest spectral power, 27 ± 1.5 min.

The MSTID propagation direction was predominately toward the NE during 2200 to 0500 UT (~0800 to 1500 MLT), and predominately toward the NW after ~0500 UT and well into the evening, possibly as late as 1400 UT (i.e., 1500 to 2400 MLT). We speculate this transition was partly caused by the radar field of view rotating about the geomagnetic pole, and coming under the influence of two separate AGW excitation regions fixed in the Sun-Earth reference frame (in a statistical sense). These excitation regions are likely related to the distribution of field-aligned currents [3], [20], [21], Poynting flux [22], and directly to the corresponding thermospheric Joule heating. That is, the major change in propagation direction was due to fore- and after-noon maxima in the distribution of field-aligned currents flowing from the magnetosphere to the ionosphere, where the associated horizontal closure currents caused Joule heating in the E region. Atmospheric gravity waves are excited, especially when the Joule heating is impulsive. In a future study, it may be possible to identify specific excitation regions using coordinated radar-satellite techniques, as outlined in [22].

However, there is a complementary explanation for the transition in MSTID direction at ~0500 UT. The observed propagation speeds of ~200 m s^{-1} are not dramatically greater than typical thermospheric wind speeds encountered at high latitudes. Hence we must consider Doppler shifting of the AGWs [23] which tends to decrease the wavelength and increase the amplitude of the waves propagating against the neutral wind. On the other hand, the AGWs tend to vanish when they propagate in the same direction as the neutral wind. However, for the latter waves that do not transfer all of their energy and momentum to the mean thermospheric flow, we might expect the spatial resonance mechanism [24] to occasionally amplify their ionospheric signatures. This is because the ionospheric drifts are often aligned with the neutral winds at high latitudes.

Consulting a model of high-latitude thermospheric winds [25] suggests the wind direction is often toward the SW (favouring propagation of AGWs toward the NE) prior to ~0500 UT, and thereafter toward the SE (favouring propagation of AGWs toward the NW). Past midnight (~1400 UT) the neutral winds become strongly equatorward, favouring propagation of AGWs toward the pole. Although this is consistent with the results shown in Fig. 6, all of the preceding hypotheses require further testing using atmospheric modeling, a SuperDARN radar supported by satellite observations of field-aligned currents, and Fabry-Perot spectrometer observations of thermospheric winds.

Acknowledgment

Longsong He acknowledges support by the International Postgraduate Research Scholarship Scheme and the La Trobe University Postgraduate Scholarship Scheme.

REFERENCES

[1] J. C. Samson, R. A. Greenwald, J. M. Ruohoniemi, and K. B. Baker, "High-frequency radar observations of atmospheric gravity waves in the high-latitude ionosphere," *Geophys. Res. Lett*., vol. 16, pp. 875-878, 1989.

[2] J. C. Samson, R. A. Greenwald, J. M. Ruohoniemi, A. Frey, and K. B. Baker, "Goose Bay radar observations of Earth-reflected atmospheric gravity waves in the high-latitude ionosphere," *J. Geophys. Res*., vol. 95, pp. 7693-7709, 1990.

[3] W. A. Bristow, R. A. Greenwald, and J. C. Samson, "Identification of high-latitude acoustic gravity sources using the Goose Bay HF radar," *J. Geophys. Res.*, vol. 99, pp. 319-331, 1994.

[4] P. L. Dyson and J. C. Devlin**,** "The Tasman International Geospace Environment Radar," *The Physicist* (The Australian Institute of Physics)*,* vol. 37, pp. 48-53, 2000.

[5] M. Tsutsui, T. Horikawa, and T. Ogawa, "Determination of velocity vectors of thermospheric wind from dispersion relation of TID's observation by an HF Doppler array," *J. Atmos. Terr. Phys.*, vol. 46, pp. 447-462, 1984.

[6] G. Crowley, T. B. Jones, and J. R. Dudeney, "Comparison of short period TID morphologies in Antarctica during geomagnetically quiet and active intervals," *J. Atmos. Terr. Phys*., vol. 49, pp. 1155-1162, 1987.

[7] T. Shibata, "Application of multichannel maximum entropy spectral analysis to the HF Doppler Data of medium-scale TID," *J. Geomagn. Geoelectr*., vol. 39, pp. 247-260, 1987.

[8] W. X. Wan, H. Yuan, and J. Liang, "An analysis method of non-uniform ionospheric disturbances from array observation," *Chinese J. Geophys*., vol. 39, pp. 183-190, 1996.

[9] G. E. Hall, J. W. MacDougall, J. F. Cecile, D. R. Moorcroft, and J. P. St.-Maurice, "Finding gravity wave source positions using the Super Dual Auroral Radar Network," *J. Geophys. Res*., vol. 104, pp. 67-78, 1999.

[10] J. W. MacDougall, D. A. Andre, G. J. Sofko, C.-S. Huang, and A. V. Koustov, "Travelling ionospheric disturbance properties deduced from Super Dual Auroral Radar Measurements," *Ann. Geophy*., vol. 18, pp. 1550-1559, 2001.

[11] R. A. Greenwald, K. B. Baker, R. A. Hutchins, and C. Hanuise, "An HF phased-array radar for studying small-scale structure in the high-latitude ionosphere," *Radio Sci*., vol. 20, pp. 63-79, 1985.

[12] W. A. Bristow and R. A. Greenwald, "Multiradar observations of medium-scale acoustic gravity waves using the Super Dual Auroral Radar Network," *J. Geophys. Res.*, vol. 101, pp. 24,499-24,511, 1996.

[13] G. G. Bowman, Movements of ionospheric irregularities and gravity waves, *J. Atmos. Terr. Phys*., vol. 30, pp. 721-734, 1968.

[14] M. L. Parkinson and P. L. Dyson, "Measurements of mid-latitude E-region, sporadic-E, and TID-related drifts using HF Doppler sorted interferometry," , *J. Atmos. Terr. Phys*., vol. 60, pp. 509-522, 1998.

[15] M. L. Parkinson, J. C. Devlin, P. L. Dyson, M. Pinnock, H. Ye, R. J. Morris, and C. L. Waters, "Statistics of TIGER HF radar echo parameters sorted according to season and the K_p index: beam 15 results," *Proceedings of the Workshop on the Applications of Radio Science*, Leura, Australia, 20-22 February, 2002 (This issue).

[16] R. L. Balthazor and R. J. Moffett, "Morphology of large-scale traveling atmospheric disturbances in the polar thermosphere," *J. Geophys. Res*., vol. 104, pp. 15-24, 1999.

[17] M. Conde, and J. Innis, "Thermospheric vertical wind activity mapped by the Dynamics Explorer-2 satellite," *The Cedar Post*, vol. 43, p. 12, September, 2001.

[18] P. L. Dyson, R. J. Norman, and M. L. Parkinson, "Ionospheric propagation modes identified using the TIGER HF radar," *Proceedings of the Workshop on the Applications of Radio Science*, Leura, Australia, 20-22 February, 2002 (This issue).

[19] G. G. Bowman, "Upper atmosphere neutral-particle density variations compared with spread-F occurrence rates at locations around the world," *J. Atmos. Terr. Phys*., vol. 10, pp. 676-682, 1992.

[20] T. Iijima and T. A. Potemra, "The amplitude distribution of field-aligned currents at northern high latitude observed by Triad", *J. Geophys. Res*., vol. 81, pp. 2165-2174, 1976.

[21] C. L. Waters, B. J. Anderson, and K. Liou, "Estimation of global field aligned currents using the Iridium system magnetometer data," *Geophys. Res. Lett*., vol. 28, pp. 2165-2168, 2001.

[22] C. L. Waters, B. J. Anderson, R. A. Greenwald, and R. J. Barnes, "Global high latitude Poynting flux from combined Iridium and SuperDARN data," *J. Geophys. Res.*, submitted for publication.

[23] J. A. Waldock and T. B. Jones, "The effects of neutral winds on the propagation of medium-scale atmospheric gravity waves at mid-latitudes," *J. Atmos. Terr. Phys*., vol. 46, pp. 217-231, 1984.

[24] J. D. Whitehead, "Ionization disturbances caused by gravity waves in the presence of an electrostatic field and background wind," *J. Geophys. Res*., vol. 76, pp. 238-241, 1971.

[25] T. J. Fuller-Rowell and D. Rees, "A three-dimensional simulation of the global dynamical response of the thermosphere to a geomagnetic substorm," *J. Atmos. Terr. Phys*., vol. 43, pp. 701-722, 1981.